Single-particle neutron states in ^{199}Hg populated in the ^{200}Hg$(d,t)^{199}$Hg reaction

E. T. Rand,[1,*] P. E. Garrett,[1,2,†] K. Yanase,[3] N. Shimizu,[4] G. C. Ball,[5] V. Bildstein,[1] C. Burbadge,[1,‡] A. Diaz Varela,[1] T. Faestermann,[6] B. Hadinia,[1,§] R. Hertenberger,[7] D. S. Jamieson,[1,‖] B. Jigmeddorj,[1,¶] A. T. Laffoley,[1] K. G. Leach,[1,**] A. D. MacLean,[1] A. J. Radich,[1] B. Rebeiro,[2,††] C. E. Svensson,[1] S. Triambak,[2] and H.-F. Wirth[7]

[1]*Department of Physics, University of Guelph, Guelph, Ontario N1G 2W1, Canada*
[2]*Department of Physics, University of the Western Cape, P/B X17, Bellville 7535, South Africa*
[3]*RIKEN Nishina Center for Accelerator-Based Science, Wako 351-0198, Japan*
[4]*Center for Computational Sciences, University of Tsukuba, Tennodai, Tsukuba 305-8577, Japan*
[5]*TRIUMF, 4004 Wesbrook Mall, Vancouver, British Columbia V6T 2A3, Canada*
[6]*Physik Department, Technische Universität München, D-85748 Garching, Germany*
[7]*Fakultät für Physik, Ludwig-Maximilians-Universität München, D-85748 Garching, Germany*

(Received 17 August 2025; accepted 17 February 2026; published 10 April 2026)

Single-particle states in ^{199}Hg have been studied with the ^{200}Hg$(d,t)^{199}$Hg reaction using 22-MeV deuterons. The reaction products were momentum analyzed using a Q3D magnetic spectrograph, and a position-sensitive cathode-strip detector located at the focal plane recorded the particle spectra. Cross sections for the population of individual states up to approximately 3-MeV excitation energy were determined, and angular distributions have been constructed. In total, 93 levels were observed, including and 52 previously unobserved levels, and spin-parity assignments made for 16 previously established levels. The results were compared with large-scale shell-model calculations that reproduce well the spectroscopic strengths for levels at low excitation energy, and the trends in the cumulative strength to high excitation energy.

DOI: 10.1103/4r6p-prgy

I. INTRODUCTION

The discovery of a nonzero electric dipole moment (EDM) outside the level predicted by the Standard Model (SM) would signal new CP-violating physics. Despite over half a century of searches with ever-increasing experimental sensitivity, no permanent particle or atomic EDM has yet been measured (for a review, see Refs. [1,2]). The limits imposed remain consistent with SM EDM predictions, which are many orders of magnitude below the current experimental reach. What continues to motivate EDM searches is the baryon asymmetry problem and the many models, such as supersymmetry and multiple-Higgs theories, that generally predict much larger EDMs than those of the SM [1]. Furthermore, the measured EDM upper limits significantly reduce the allowed parameter spaces of these models. To date, the measured ^{199}Hg EDM, $d_{\rm Hg} = (2.20 \pm 2.75_{\rm stat} \pm 1.48_{\rm syst}) \times 10^{-30}$ $e$cm which places an overall upper limit of $|d_{\rm Hg}| < 7.4 \times 10^{-30}$ $e$cm at the 95% confidence level, provides the most stringent limit on an EDM [3]. However, as outlined in Ref. [1], the measurements of EDMs in different systems provide sensitivity to different mechanisms; diamagnetic atoms like ^{199}Hg are sensitive to purely hadronic sources of the EDM arising from the odd-neutron (d_n in the case of ^{199}Hg) and the QCD parameter $\bar{\theta}$ that sets the scale of CP violation in the strong interaction. Paramagnetic systems, on the other hand, provide more sensitivity to the electron EDM d_e as well as the scalar electron-nucleon interaction coefficient (C_s) arising from the effective field theory approach involving quark-gluon interactions [1]. Thus, EDM searches must be conducted on a variety of systems to fully understand the underlying mechanism.

In an atomic system like ^{199}Hg, it is the Schiff moment [4] of the nucleus that generates the observable EDM in the electron cloud of the atom. The Schiff moment measures the difference between the charge and the electric dipole distributions within the intrinsic frame of the nucleus and is the lowest order time-odd nuclear moment that is measurable in a neutral atom [5]. Octupole-deformed nuclei are predicted to have large Schiff moments due to existence of close-lying parity doublets, resulting in an increased sensitivity to P and T-odd violations by factors of 100 to 1000 relative to ^{199}Hg [6–8]. It was suggested [9], however, that the Schiff moment in ^{199}Hg

*Present address: Canadian Nuclear Laboratories, Chalk River, ON, Canada.
†Contact author: pgarrett@physics.uoguelph.ca
‡Deceased.
§Present address: Candu Energy Inc.
‖Present address: Max Planck Institute for Astrophysics, 85748 Garching, Germany.
¶Present address: School of Natural Science, Laurentian University, Sudbury, ON, Canada.
**Present address: Department of Physics, Colorado School of Mines, Golden, CO, USA.
††Present address: GANIL, Bd Henri Becquerel, 14076 Caen Cedex 05, France.

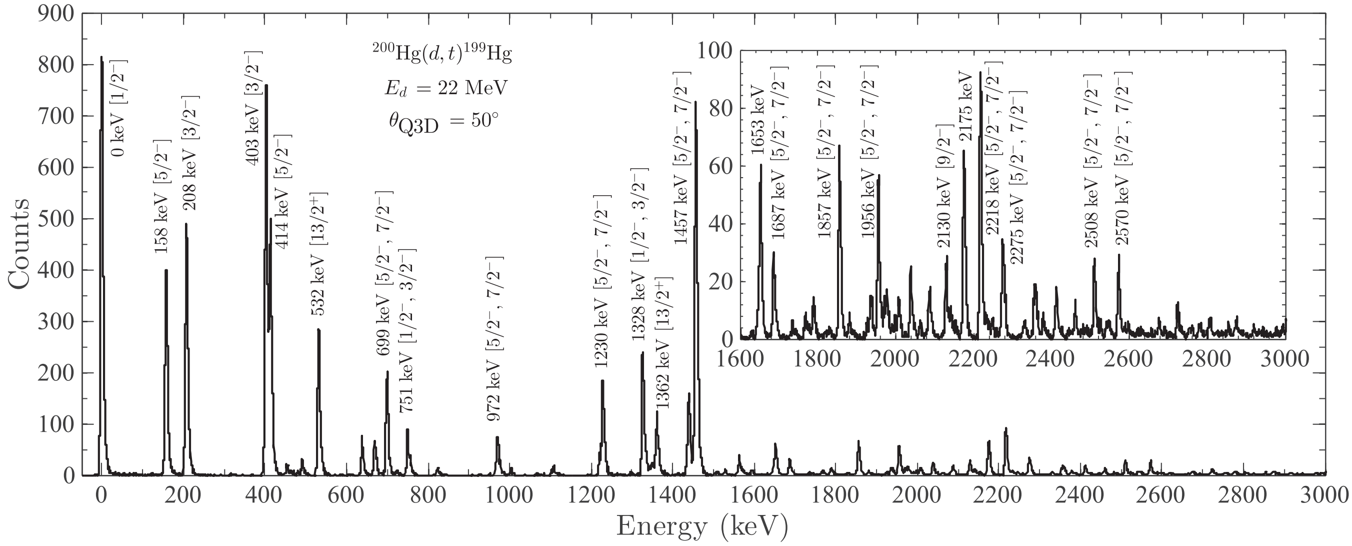

FIG. 1. Spectrum of observed tritons from the (d, t) single-neutron pickup reaction on ^{200}Hg at a laboratory angle of 50°. The inset shows an expanded portion of the spectrum in the region of 1.6–3.0 MeV to illustrate the level of detail in the higher-lying levels.

could be larger than early calculations reported, resulting in less dramatic enhancement factors for octupole-deformed nuclei when compared to ^{199}Hg.

Theoretical calculations of the Schiff moment in ^{199}Hg are challenging, in part due to insufficient detail of the nuclear-structure information. Very recently, large-scale shell-model calculations of the nuclear Schiff moment of ^{199}Hg were performed [10]. In the present work, we report on results of a single-nucleon transfer study, using the ^{200}Hg(d, t) reaction, in order to probe the single-particle neutron configurations present in the states in ^{199}Hg, and compare the results with predictions of this large shell-model calculation.

II. EXPERIMENT

The experiments were conducted at the Maier-Leibnitz Laboratory in Garching, Germany, on the campuses of the Ludwig-Maximilians Universität and the Technische Universität München as part of a program to study both the single-neutron transfer as well as the ^{200}Hg(d, d') inelastic-scattering reaction. The 14-MV Tandem Van de Graaff accelerator provided a 22-MeV deuteron beam incident on isotopically enriched targets of ^{200}Hg$\,^{32}$S, with a mercury isotopic enrichment >98%, and ^{32}S enriched to >99%. The mercury-sulphide targets were approximately 100 μg/cm^2 thick, with two foils of approximately 10 μg/cm^2 of natural carbon forming sandwiching layers over the HgS. The deuteron beam current was limited to <1 μA, although some measurements were taken with much lower beam currents.

The (d, t) single-nucleon transfer reaction on ^{200}Hg was performed at ten angles from 5° to 50°, in increments of 5°. The reaction products were momentum analyzed using the Q3D magnetic spectrograph, where the resulting particles were detected at the focal plane using a position-sensitive detector [11]. The focal-plane detector consisted of two proportional counters backed by a thick plastic scintillator. The first proportional counter had a single anode wire that registered the signal ΔE_1. The second proportional counter had two anode wires which registered signals that were summed to produce ΔE_2 and is furthermore coupled with a position-sensitive cathode strip foil. A thick plastic scintillator placed behind the proportional counters was sufficiently thick to stop the particles providing a signal proportional to the total energy E (minus the two ΔEs). Particle identification was achieved through gating conditions placed on the $\Delta E_2 - \Delta E_1$ and $\Delta E_2 - E$ two-dimensional histograms. A typical spectrum of the observed tritons from the (d, t) pickup reaction on ^{200}Hg is shown in Fig. 1. The energy resolution achieved for the particle energy spectra was 7- to 8-keV full width at half maximum.

It was found early in the campaign that beam currents of several hundred nanoamperes would result in an apparent change in target thickness. This was attributed to localized migration of Hg material, likely due to melting of the HgS, characterized by a drop of the counting rate of peaks from Hg over a period of several minutes following the commencement of beam on target. Corresponding drops in count rates due to other target impurities, and the sulfur, were not observed. It was also observed that the Hg peak count rate recovered to its initial value following a several minute period of no beam irradiation of the target. In order to overcome this changing effective target thickness, we followed the practice of ensuring that peaks in common to the spectra taken with different momentum settings of the spectrograph always had sufficient counts to guarantee a mutual normalization of the spectra with a relative precision of better than 3%. Thus, all spectra for spectrograph settings for excited states could be renormalized to the momentum setting that covered the ground-state region. The large cross sections observed for the peaks in the spectra containing the ground-state permitted data to be collected using low beam currents thereby minimizing the Hg migration effect. Figure 2 displays the measured angular distribution for the ^{199}Hg ground state, known to be a $1/2^-$ state, that is populated with an $\ell = 1$

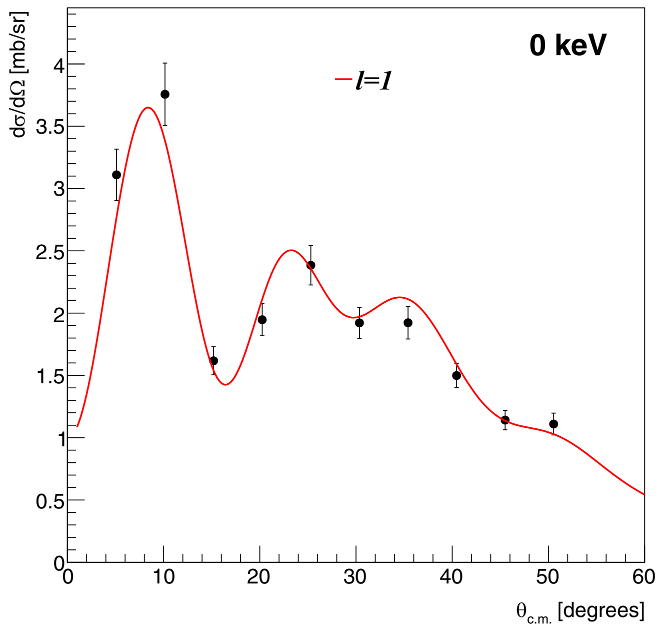

FIG. 2. Measured cross sections and calculated angular distribution for the ^{199}Hg ground state. The curve is the result of a DWBA calculation for an $\ell = 1$ transfer (see text for details). A spectroscopic strength of 1.49 was extracted through a least-squares fit to the experimental data.

transfer from the $I = 0^+$ ^{200}Hg target. Also displayed on the figure is the angular distribution from distorted-wave Born approximation (DWBA) calculations (described below) that shows excellent agreement with the experimental data, providing confidence in the relative normalizations. The target thicknesses were obtained from the elastic scattering on the ^{200}Hg ground state where data were collected using a similar current-limiting procedure and in a series of very short measurements, typically of 5-min duration. The data from these short normalization runs were then compared with the DWBA calculations of the elastic-scattering cross sections which also showed excellent agreement (see Sec. III A). The nominal target thicknesses were determined through normalization of the experimental deuteron elastic-scattering cross section to the DWBA prediction at 20° where Coulomb scattering is dominant and there is little sensitivity to reaction model parameters.

In order to ensure reliability of the results, during the course of the experiment repeated consistency checks were made to ensure that the target thickness remained constant. This encompassed returning the spectrograph to a selected angle and magnetic setting and repeating the data collection. This procedure determined a value for the beam current that would result in the reproduction of the cross section to within a few percentages. With the absolute cross sections determined for peaks in spectra containing the ground state, the beam current for the spectra collected at the magnetic field settings for the higher excitation energy region could be increased in order to have reasonable statistics for the weakly populated states, such as those shown in the inset in Fig. 1.

A. Target impurities

A detailed investigation into possible target impurities and contaminants was performed in order to eliminate the possibility of introducing spurious levels in ^{199}Hg. Target contaminants were categorized into two mass ranges; low- and high-mass contaminants. The low-mass contaminants include those arising from the natural carbon backing, (^{12}C and ^{13}C), the isotopically enriched sulfur (^{32}S), and atmospheric contaminants that are present in the target (^{14}N, ^{16}O, etc.). The high-mass contaminants include the isotopic impurities from the mercury isotope separation process ($^{196-199,201-204}$Hg), and any other impurities with a mass around $A = 200$ and may have been introduced during the target making process.

Peaks arising from reactions on low-mass contaminants were easily identifiable in the resulting triton focal-plane spectra. These peaks are kinematically broadened, and appeared as wide, irregularly shaped peaks compared to the narrower peaks of interest from the ^{200}Hg$(d,t)^{199}$Hg reaction that were focused on the focal plane. Additionally, the relative positions of these peaks shift as a function of laboratory angle. This dynamic feature results in gaps in the cross-section angular distributions of the peaks assigned to ^{199}Hg. Peaks arising from reactions on high-mass contaminants are generally indistinguishable from those of the primary reaction of interest due to their similar masses. Using the known reaction Q values, however, peaks arising from the known Hg isotopic impurities were sought, but none could be positively identified consistent with the level expected from the observed spectra from an independent (d,d') reaction (see Fig. 1 of Ref. [12]).

B. Energy calibration

The spectra acquired on the focal plane of the spectrograph display a nonlinear dependence of energy as a function of position. The nonlinear energy dependence is a polynomial up to an order of 3 [13]. Fortunately, many states in ^{199}Hg are well determined from high-resolution γ-ray spectroscopy measurements [14], providing a set of energy calibration points for the triton focal-plane spectra. Figure 3 illustrates energy calibrations for the high- and low-momentum settings for the magnetic field of the spectrograph. These momentum settings covered an energy range up to approximately 3-MeV excitation energy and overlapped by approximately 300 keV from ∼1.4 to 1.7 MeV. The MINUIT2 libraries [15] were used to extract the fit parameters through χ^2 minimization. A statistical F_χ test [16] on the energy calibration of the triton focal-plane spectra demonstrated that a polynomial of order 2 was satisfactory at a 95% level of significance.

C. Cross-section measurements

The FitPic software package [17] was used to fit the observed peaks in the focal-plane spectra and peak areas were extracted. Experimental cross sections were calculated for each angle and momentum setting via the relation

$$\frac{d\sigma}{d\Omega} = \frac{N_c}{N_{t,\mathrm{eff}}\, N_b\, d\Omega\, LT}, \qquad (1)$$

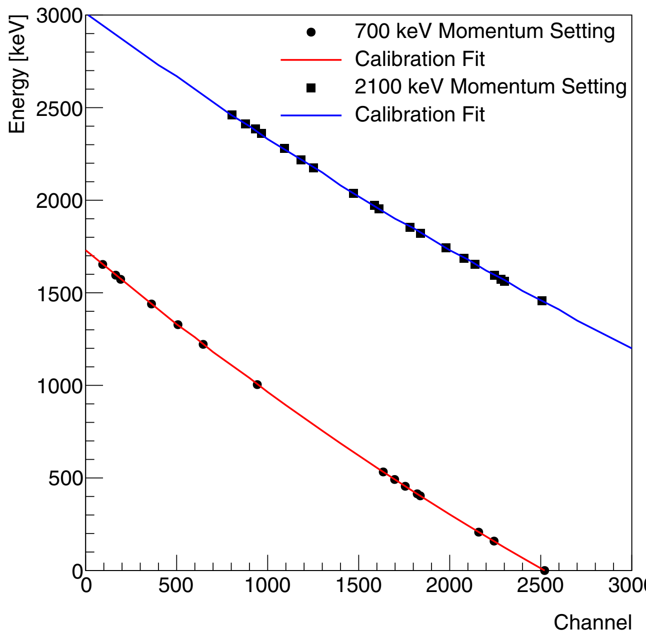

FIG. 3. Energy calibrations for the high- and low-momentum settings used for the magnetic spectrograph for the ^{200}Hg(d,t) reaction. Calibration points are from known states in ^{199}Hg [14]. Error bars in both the x and y are too small to observe and were therefore not included in the plot.

where N_c is the number of counts in the peak, $N_{t,\mathrm{eff}}$ is the effective target thickness that takes into account the rotation of the target with respect to the incident beam (the outgoing tritons were perpendicular to the target surface in order to minimize energy straggling), N_b is the integrated number of beam particles incident on the target, $d\Omega$ is the solid-angle acceptance of the Q3D, and LT is the live-time correction for both the focal-plane detector and data acquisition system. The number of beam particles was monitored by a Faraday cup placed at 0° behind the target with the current integrated by a Brookhaven Instruments Corporation current integrator with the output sent to a scalar. The data acquisition (DAQ) dead time was determined using a second scalar to count the pulses from the current integrator in coincidence with the DAQ dead-time pulses. The application-specific integrated circuits of the focal plane detector also provided signals used to determine their dead times. For most of the present (d,t) measurements the combined dead times were only a few percentages.

The uncertainties on the cross sections include the statistical uncertainties arising from the peak areas, including the normalization procedure described above where applicable. An additional 3% uncertainty was applied to account for uncertainties in the target thickness determination, taking into account those associated with the current integration and dead-time corrections.

III. DWBA CALCULATIONS AND EXTRACTED SPECTROSCOPIC FACTORS

Angular distributions of the differential cross sections for each level are shown in Figs. 6, 7, and 8. The code FRESCO [18,19] was used to perform finite-range DWBA calculations with various global optical model potential (OMP) parameter sets. The spectroscopic strengths $S_{\ell j}$ were extracted via

$$\left.\frac{d\sigma}{d\Omega}\right|_{\mathrm{EXP}} = S_{\ell j}\left.\frac{d\sigma}{d\Omega}\right|_{\mathrm{DWBA}}. \qquad (2)$$

The optical model potential in these calculations was given by

$$V(r) = -V_r f_r(r) - iW_v f_v(r) + i4a_s W_s \frac{df_s(r)}{dr} + \lambda_\pi^2 \frac{V_{\mathrm{so}} + W_{\mathrm{so}}}{r}\frac{df_{\mathrm{so}}(r)}{dr}(2\vec{l}\cdot\vec{s}) + V_C(r), \qquad (3)$$

where f_i was given as a Woods-Saxon potential

$$f_i(r, R_i, a_i) = \left[1 + \exp\left(\frac{r - R_i}{a_i}\right)\right]^{-1}, \qquad (4)$$

and where $i = r, v, s$, and so are the real volume, imaginary volume, imaginary surface, and spin-orbit terms, respectively. The nuclear radius is $R_i = r_i A^{(1/3)}$ and a_i is the diffuseness of the potential.

A. Deuteron OMP parameter sets

Elastic scattering of 22-MeV deuterons on ^{200}Hg was measured for 21 angles, from 15° to 115°, in steps of 5°. Four global deuteron OMP parameter sets were investigated: Daehnick, Childs, and Vrcelj [20], An and Cai [21], Bojowald *et al.* [22], and Han, Shi, and Shen [23]. All tested deuteron OMP parameter sets reproduced the deuteron elastic scattering exceptionally well as shown in Fig. 4 except that of Bojowald *et al.* [22]. The Daehnick, Childs, and Vrcelj deuteron OMP parameter set was chosen as the optimal set and was used in analysis on the basis that it provided the best reproduction of the elastic-scattering data. The adopted OMP parameters for 22-MeV deuterons on ^{200}Hg are given in Table I.

B. Triton OMP parameter sets

Triton elastic-scattering data on isotopes of mercury are not available. The set of data that most closely matches our experimental conditions of the outgoing tritons was sought via the Experimental Nuclear Reaction Data database [25,26] and was found to be the scattering of 33-MeV tritons on ^{208}Pb [27]. In addition to the lack of available triton scattering data, there are also fewer global OMP parameter sets in the literature. Two global triton OMP parameters sets were investigated: Li, Liang, and Cai [24] and Pang *et al.* [28]. While neither of the global sets reproduced the cross sections accurately for large angles, as shown in Fig. 5, the set by Li, Liang, and Cai [24] was judged to reproduce the experimental data better and therefore was used as the optimal global OMP parameter set in the analysis.

C. Neutron OMP parameters

Two sets of OMP parameters were used for the binding of the neutron in the ^{200}Hg and for the binding of the neutron in the triton. For the former, we used the Woods-Saxon potential

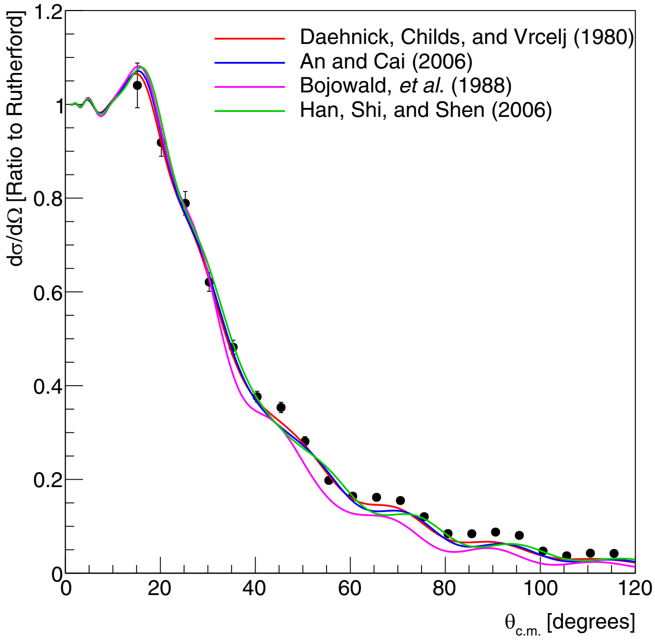

FIG. 4. Experimental elastic-scattering cross sections plotted as a ratio to Rutherford scattering for 22-MeV deuterons on ^{200}Hg. The DWBA curves for four global OMP parameter sets are shown: Daehnick, Childs, and Vrcelj [20], An and Cai [21], Bojowald *et al.* [22], and Han, Shi, and Shen [23]. The global OMP parameter set that best reproduces the experimental data is given by Daehnick, Childs, and Vrcelj [20].

of Koning and Delaroche [29] but take the real part of the potential only and with the volume depth adjusted to reproduce the neutron binding energies of the target. A spin-orbit component was also included. For the bound neutron in the triton, we took recommended [30] values from Ref. [31] where the real depth was also adjusted to reproduce the binding energy of 6.257 MeV. The numerical values of the parameters used are given in Table II.

D. Uncertainties on S_{jl}

In order to address the systematic error associated with the choice of OMP parameter sets, all possible combinations of the deuteron and triton OMP parameter sets discussed above were considered in the calculation of the spectroscopic factors. It was found that a model dependency systematic error of 15% was appropriate when comparing the resulting spectroscopic factors. Using the deuteron OMP parameter set by Bojowald *et al.* [22] resulted in the largest deviations in the calculated of spectroscopic factors compared to the calculations with the adopted deuteron and triton OMP parameter sets by Daehnick and Childs [20] and Li, Liang, and Cai [24], respectively. Using the adopted triton OMP parameter set, the calculated spectroscopic factors deviated up to 18% for the 32 lowest energy levels. When using the triton OMP set by Pang *et al.* [28], these spectroscopic factors deviated up to 29%, with a combined average deviation of 15%. Due to the poor reproduction of the experimental elastic cross sections, the Bojowald *et al.* OMP parameter set was removed from the systematic error analysis. The remaining deuteron OMP parameter sets (by An and Cai [21] and Han, Shi, and Shen [23]) yielded much smaller deviations in the spectroscopic factors with an average deviation of 8% observed. In addition,

TABLE I. Values for the OMP parameters used in the present analysis. The triton parameters V_r and W_s were calculated as a function of triton energy (E_T). Potential well depths are given in units of megaelectronvolts, and reduced radii and diffuseness parameters are in units of femtometers.

Parameter	Deuteron (Daehnick, Childs, and Vrcelj [20])	Triton (Li, Liang, and Cai [24])
r_C (fm)	1.3	1.4219
V_r (MeV)	94.8182	$0.4360E_T^2 - 0.1456E_T + 186.8304$
r_r (fm)	1.17	1.0943
a_r (fm)	0.7464	0.7948
W_v (MeV)	0.6034	$-0.0097E_T^2 + 0.5025E_T + 7.3830$
r_v (fm)	1.325	1.2898
a_v (fm)	0.9394	1.2307
W_s (MeV)	12.1686	$-0.6451E_T + 27.8117$
r_s (fm)	1.325	1.1718
a_s (fm)	0.9394	0.8791
V_{so} (MeV)	3.346	1.9029
r_{so} (fm)	1.07	0.4921
a_{so} (fm)	0.66	0.0497
W_{so} (MeV)	0.0	0.0

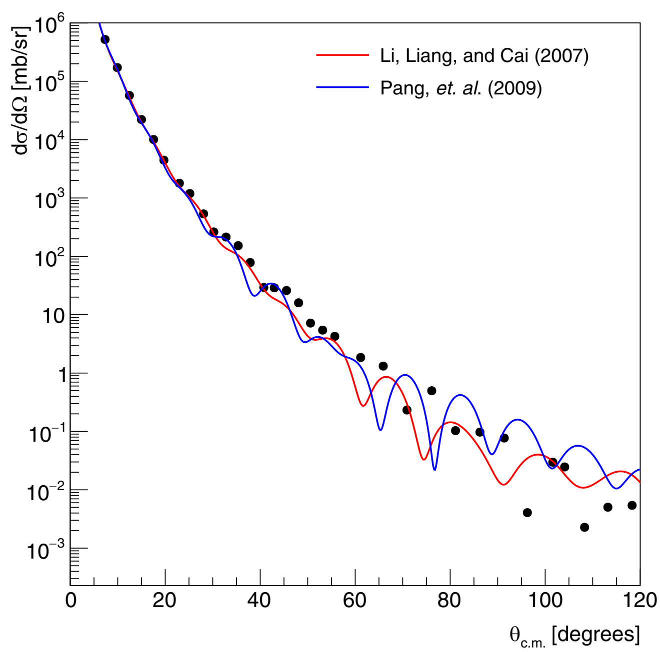

FIG. 5. Experimental elastic-scattering cross sections for 33 MeV tritons on ^{208}Pb from England *et al.* [27]. The DWBA curves for two global OMP parameter sets are shown: Li, Liang, and Cai [24] and Pang *et al.* [28]. The global OMP parameter set that best reproduces the experimental data is given by Li, Liang, and Cai [24].

TABLE II. Values for the neutron OMP parameters used in the present analysis. Potential well depths are given in units of megaelectronvolts, and reduced radii and diffuseness parameters are in units of femtometers. The real depths listed are those that reproduce the neutron binding energy for the ^{3}H and ^{200}Hg ground states.

Parameter	n binding potential in ^{3}H [30,31]	n binding potential in ^{200}Hg [29]
V_r	87.3	44.7
r_r	0.95	1.2345
a_r	0.65	0.6482
V_{so}	0	6.09
r_{so}		1.0746
a_{so}		0.590

spectroscopic factors deduced using DWBA calculations with the DWUCK4 code [32] were also investigated. Using the recommended normalization and finite range parameters, the calculated spectroscopic factors deviated less than 7% compared to the FRESCO calculations. This comparison was done for various p, f, and i shell transfers.

It was determined that the OMP parameter set dependency was the largest systematic effect. From the above investigations, it is recommended that the spectroscopic factors reported in this work have an additional 15% systematic uncertainty from the choice of OMP parameter set and reaction model. This 15% systematic uncertainty is not included in the uncertainties reported in Table III.

IV. RESULTS

Many of the states observed in ^{199}Hg from the (d,t) pickup reaction on ^{200}Hg have been previously identified from the pickup and stripping reactions performed by Moyer [33] or through other reactions and decays [14]. Observed levels for which there is new information, such as the transferred ℓ value, are discussed below.

A total of 91 peaks were observed, of which two are due to unresolved doublets of levels and assigned as states of ^{199}Hg populated in the reaction. Figures 6, 7, and 8 display the cross-section angular distributions observed for the peaks, together with the FRESCO calculations for the assigned transferred ℓ values. Table III gives the list of observed levels, spin-parity assignments, and spectroscopic factors.

A. New levels in ^{199}Hg

From the 91 observed peaks in this work, 52 new levels were identified. The consistency of the position of the peaks across many angles provided confidence in the existence of these new states. Furthermore, 22 of these peaks yielded distinct angular distributions allowing the assignment of the transferred ℓ value. This ℓ value provided firm parity assignments and spin assignments based on $j = \ell \pm 1/2$. In some cases, if the transferred ℓ value could only arise from one of the spin-orbit partners in the vicinity of the Fermi level, then that spin was adopted. We use this assumption for the observed high-ℓ transfers with $\ell = 5$ ($h_{9/2}$) and $\ell = 6$ ($i_{13/2}$). The remaining 28 peaks had angular distributions that were either incomplete, or much smaller cross sections, and therefore an ℓ-value and spin-parity assignment could not be conclusively determined. Below, we discuss only a few select levels.

For cases where we could not make a specific J^π assignment, the calculation of the spectroscopic strength used the form factor calculated with the $\ell - 1/2$ single-particle orbital. This generally results in an insignificant change to the extracted spectroscopic strength. For example, if calculations are repeated for the ground state assuming a $p_{3/2}$ transfer instead of a $p_{1/2}$ transfer, then S changes from 1.49 to 1.48. A very similar result is obtained for $\ell = 3$ transfers. Some of the angular distributions have insufficient detail to permit the extraction of the transferred-ℓ values; for those no spectroscopic strengths are reported.

1. Low-lying levels at 467 and 482 keV

Two new states below 500 keV were identified in the present work, at 467 and 482 keV. These two levels lie close in energy to neighboring, and previously known, levels at 455 and 492 keV, respectively. The cross sections of the new levels are approximately an order of magnitude smaller than the neighboring levels, which would have made it difficult to observe in the previous lower-resolution transfer reaction studies performed by Moyer [33].

The DWBA analysis for the 467-keV level is consistent with an $\ell = 1$ transfer, assigning the spin-parity of this level as $\frac{1}{2}^-$ or $\frac{3}{2}^-$. The cross-section measurements at 5° and 10° could not be determined for the level at 482 keV due to the presence of a small impurity peak in the spectra. The remaining angles lack a strong signature in the resulting angular distribution to confidently assign the ℓ transfer, although the level appears to be dominated by an $\ell = 1$ transfer, similarly to the 455- and 492-keV levels, indicating a $J^\pi = \frac{1}{2}^-$ or $\frac{3}{2}^-$ assignment.

2. 640-keV level

A level observed at 640 keV in the previous (d,t) transfer reaction experiments by Moyer [33] lacked an assigned ℓ transfer value and hence an uncertain spin-parity assignment. In the present work, the angular distribution has a pattern that favors $\ell = 3$ over that of $\ell = 1$, implying an $2f_{\frac{5}{2},\frac{7}{2}}$ component, similarly to the neighboring 699-keV level. We thus assign the spin-parity of this level as $\frac{5}{2}^-$ or $\frac{7}{2}^-$.

3. 711-keV level

A level at 711 keV was postulated to exist from results of the ^{198}Hg(n,γ) reaction [34]. In the present study, no evidence is found for this level. While nonobservation in the (d,t) reaction cannot be taken as proof of its nonexistence, we note this level was established via a primary γ-ray from the capture state, and no secondary γ-ray decays have been assigned.

4. 723-keV level

A new level is observed at 723 keV, with the population cross section approximately an order of magnitude lower than

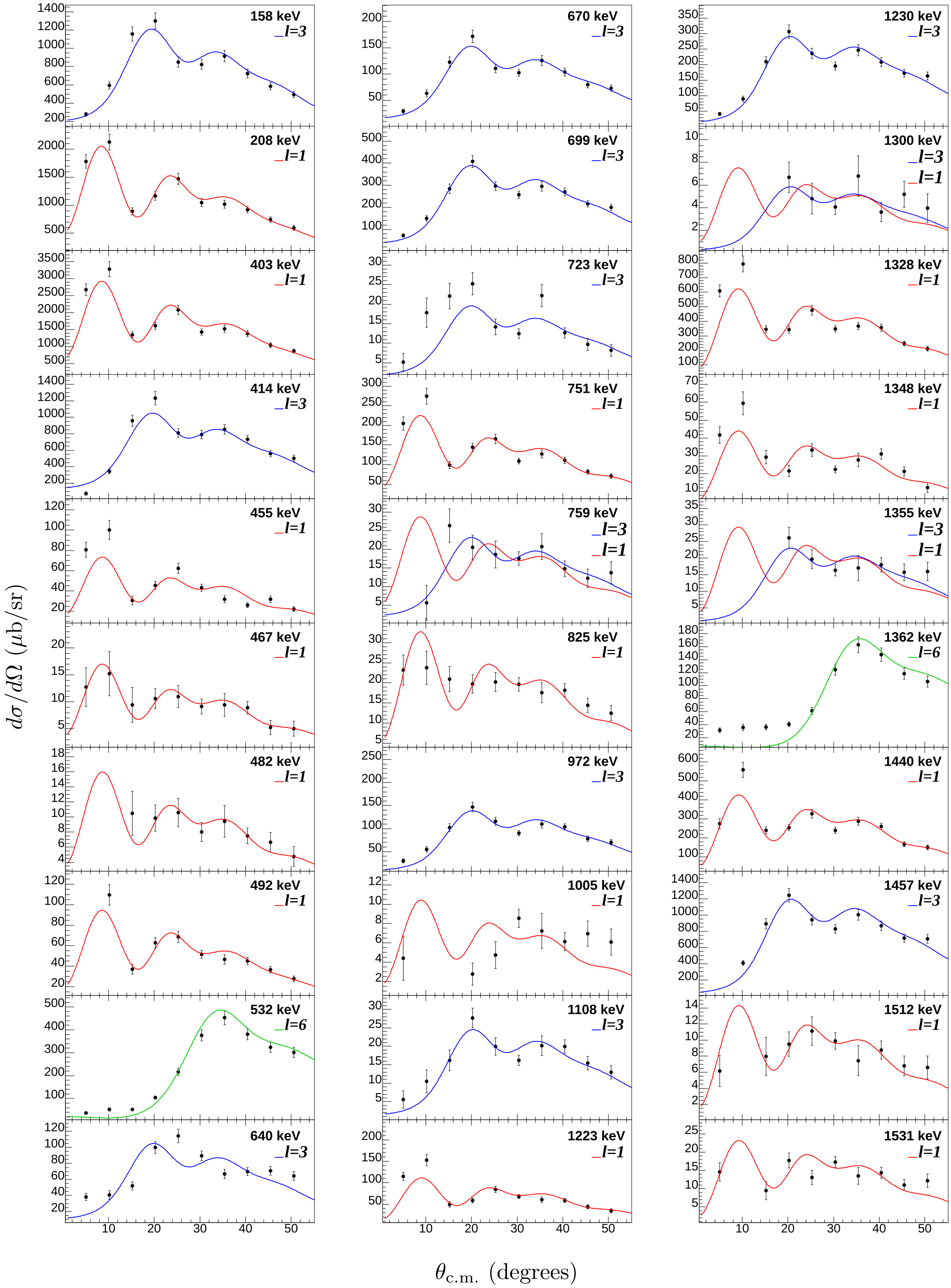

FIG. 6. Measured cross sections and calculated angular distributions for states populated in the ^{200}Hg$(d,t)^{199}$Hg reaction in the excitation energy range of 0 to 1.53 MeV. The angular distribution curves are the result of DWBA calculations for the indicated transferred ℓ values. Spectroscopic strengths were extracted through χ^2 minimization fits to the experimental data. Multiple transferred ℓ value fits are shown for states where the J^π information was uncertain and a single fit did not sufficiently reproduce the experimental data.

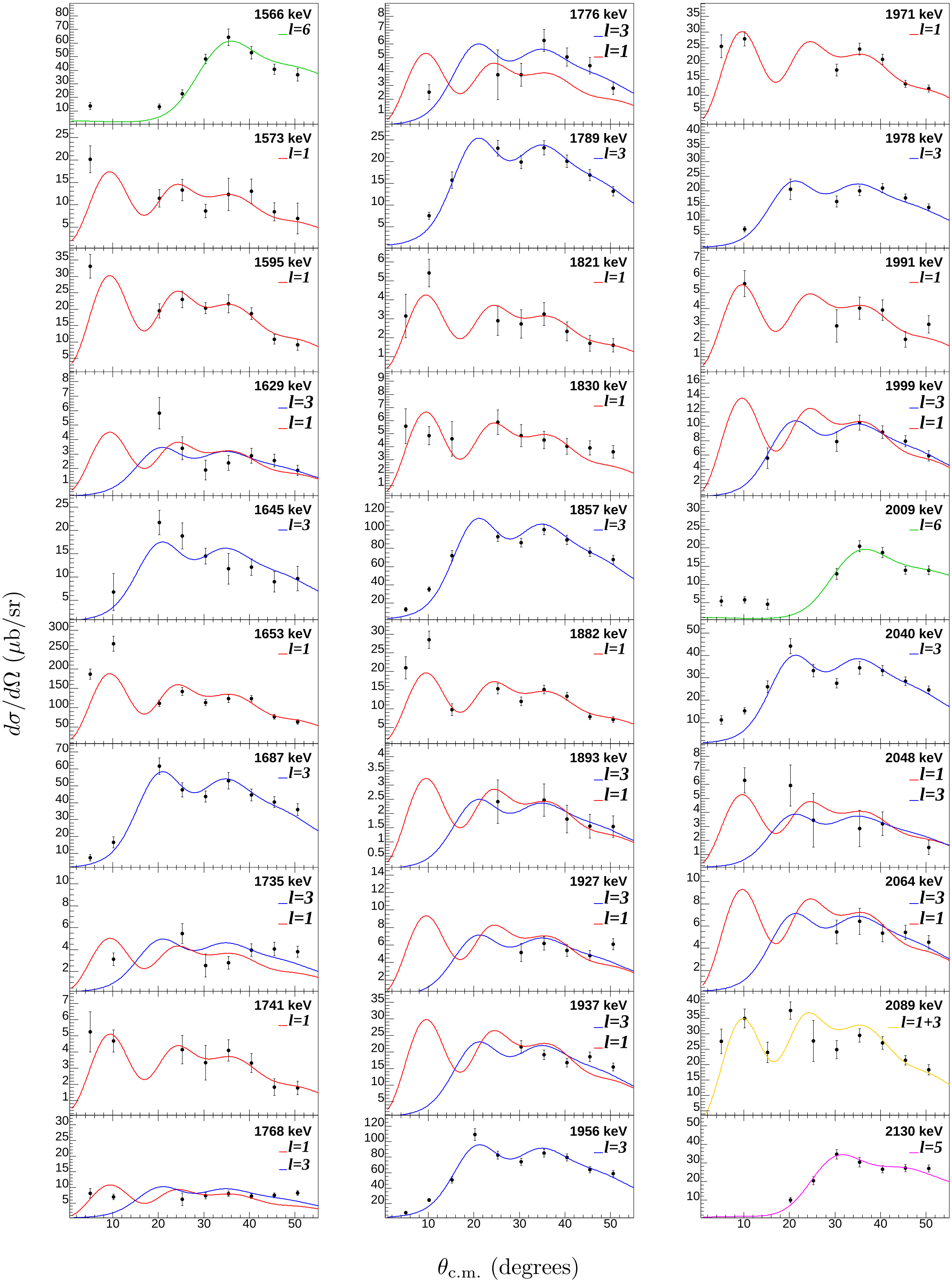

FIG. 7. Measured cross sections and calculated angular distributions for states populated in the ^{200}Hg$(d,t)^{199}$Hg reaction in the excitation energy range of 1.57 to 2.13 MeV. See caption to Fig. 6 for details.

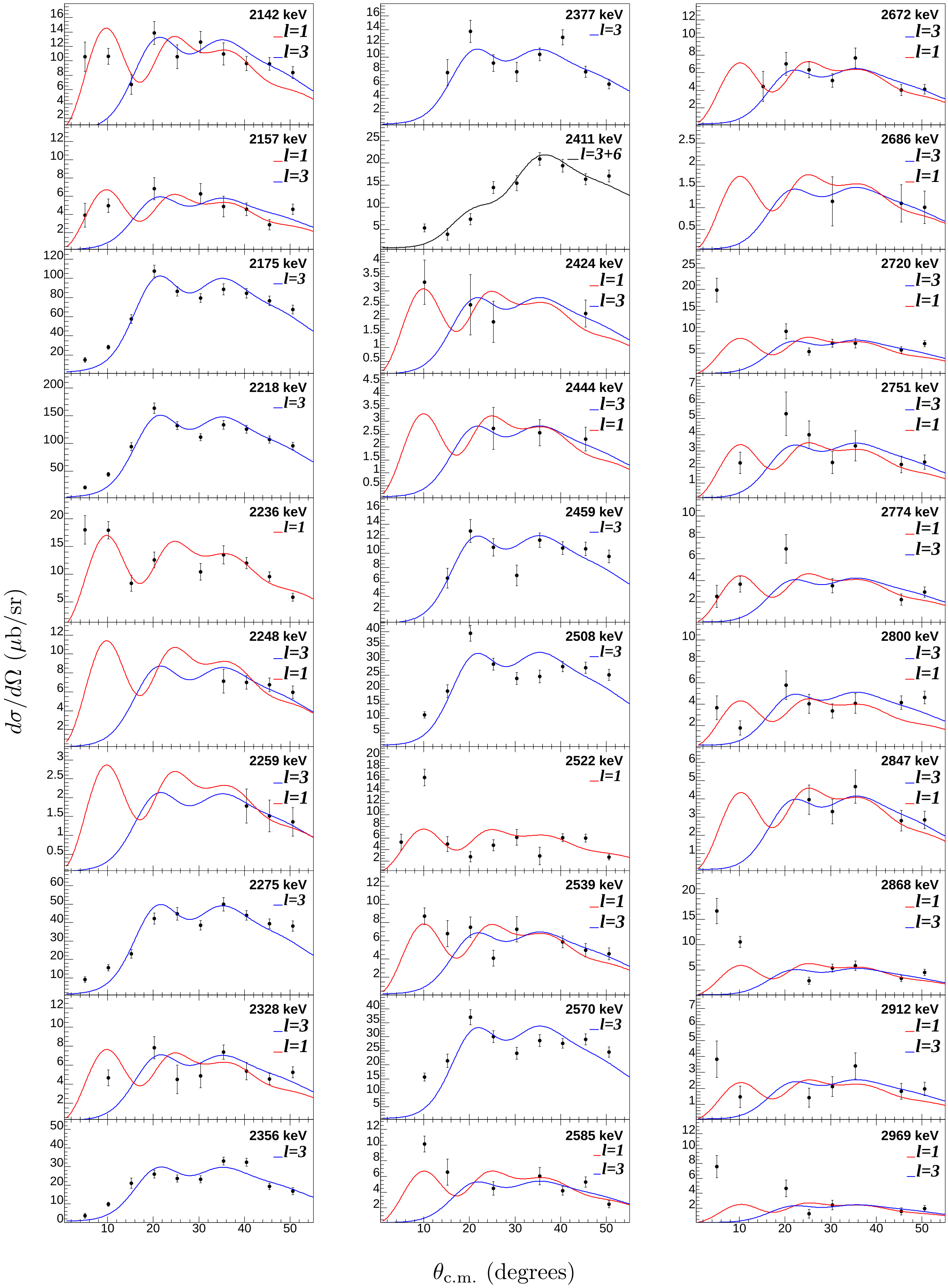

FIG. 8. Measured cross sections and calculated angular distributions for states populated in the ^{200}Hg(d,t)^{199}Hg reaction in the excitation energy range of 2.14 to 2.97 MeV. See caption to Fig. 6 for details.

TABLE III. Results obtained from the ^{200}Hg$(d,t)^{199}$Hg reaction with 22-MeV deuterons. The excitation energies are obtained from the calibration polynomials described in Sec. II B. The uncertainties on the cross sections include statistical errors arising from the peak areas, an uncertainty in the solid angle of the Q3D aperture, and a 3% systematic uncertainty estimated on the target thickness normalization. Spectroscopic strengths are obtained from the FRESCO calculations described in the text. Uncertainties on the strengths are statistical only and do not include a recommended 15% systematic uncertainty due to the choice of the optical model parameters and reaction model.

E_{exp} (keV)	J^{π}_{exp}	$d\sigma/d\Omega\|_{max}$ (mb/sr)	$n\ell_j$	$S_{\ell j}$
0	$1/2^-$	3.8(3)	$3p_{\frac{1}{2}}$	1.49(3)
158.0(1)	$5/2^-$	1.3(9)	$2f_{\frac{5}{2}}$	1.74(4)
207.8(1)	$3/2^-$	2.1(1)	$3p_{\frac{3}{2}}$	0.78(2)
403.1(1)	$3/2^-$	3.3(2)	$3p_{\frac{3}{2}}$	1.04(2)
413.6(1)	$5/2^-$	1.23(8)	$2f_{\frac{5}{2}}$	1.43(3)
455.1(4)	$1/2^-, 3/2^-$	0.1(9)	$3p_{\frac{1}{2}}$	0.0254(8)
466.7(9)	$1/2^-, 3/2^-$	0.015(4)	$3p_{\frac{1}{2}}$	0.0059(4)
482.1(9)	$(1/2^-, 3/2^-)$	0.011(2)	$3p_{\frac{1}{2}}$	0.0055(4)
492.2(3)	$3/2^-$	0.11(1)	$3p_{\frac{3}{2}}$	0.033(1)
532.4(2)	$13/2^+$	0.45(3)	$1i_{\frac{13}{2}}$	9.5(2)
639.6(3)	$5/2^-, 7/2^-$	0.114(8)	$2f_{\frac{5}{2}}$	0.136(4)
669.7(2)	$5/2^-, 7/2^-$	0.17(1)	$2f_{\frac{5}{2}}$	0.198(5)
699.4(2)	$5/2^-, 7/2^-$	0.41(3)	$2f_{\frac{5}{2}}$	0.50(1)
722.8(4)	$5/2^-, 7/2^-$	0.025(3)	$2f_{\frac{5}{2}}$	0.025(1)
750.7(2)	$1/2^-, 3/2^-$	0.27(2)	$3p_{\frac{1}{2}}$	0.071(2)
758.6(7)	$5/2^-, 7/2^-$	0.026(4)	$2f_{\frac{5}{2}}$	0.030(2)
824.6(5)	$1/2^-, 3/2^-$	0.024(4)	$3p_{\frac{1}{2}}$	0.0101(4)
971.7(3)	$5/2^-, 7/2^-$	0.15(1)	$2f_{\frac{5}{2}}$	0.169(4)
1004.8(9)	$1/2^-, 3/2^-$	0.0086(9)	$3p_{\frac{1}{2}}$	0.0030(2)
1108.3(5)	$5/2^-, 7/2^-$	0.028(3)	$2f_{\frac{5}{2}}$	0.029(1)
1223.0(5)	$1/2^-, 3/2^-$	0.15(1)	$3p_{\frac{1}{2}}$	0.0304(9)
1229.5(3)	$5/2^-, 7/2^-$	0.31(2)	$2f_{\frac{5}{2}}$	0.338(8)
1300(1)	$1/2^-$–$7/2^-$	0.007(2)	$2f_{\frac{5}{2}}$	0.0067(6)
1327.9(3)	$1/2^-, 3/2^-$	0.79(5)	$3p_{\frac{1}{2}}$	0.166(4)
1347.8(7)	$1/2^-, 3/2^-$	0.059(6)	$3p_{\frac{1}{2}}$	0.0116(4)
1355(1)	$(5/2^-, 7/2^-)$	0.026(3)	$2f_{\frac{5}{2}}$	0.026(1)
1362.0(4)	$13/2^+$	0.16(1)	$1i_{\frac{13}{2}}$	3.14(9)
1439.9(4)	$1/2^-, 3/2^-$	0.56(4)	$3p_{\frac{1}{2}}$	0.110(3)
1457.2(4)	$5/2^-, 7/2^-$	1.24(8)	$2f_{\frac{5}{2}}$	1.33(3)
1512(1)	$1/2^-, 3/2^-$	0.011(2)	$3p_{\frac{1}{2}}$	0.0036(2)
1531(1)	$1/2^-, 3/2^-$	0.018(2)	$3p_{\frac{1}{2}}$	0.0059(3)
1565.5(7)	$13/2^+$	0.064(6)	$1i_{\frac{13}{2}}$	1.10(4)
1573(2)	$1/2^-, 3/2^-$	0.02(3)	$3p_{\frac{1}{2}}$	0.0044(3)
1595.2(9)	$1/2^-, 3/2^-$	0.033(4)	$3p_{\frac{1}{2}}$	0.0075(3)
1629(2)	$(5/2^-, 7/2^-)$	0.006(1)	$2f_{\frac{5}{2}}$	0.0038(3)
1645(1)	$5/2^-, 7/2^-$	0.022(3)	$2f_{\frac{5}{2}}$	0.019(1)
1652.5(6)	$1/2^-, 3/2^-$	0.26(2)	$3p_{\frac{1}{2}}$	0.046(1)
1686.6(7)	$5/2^-, 7/2^-$	0.062(5)	$2f_{\frac{5}{2}}$	0.063(2)
1735(2)		0.0055(9)		
1741(3)	$1/2^-, 3/2^-$	0.005(1)	$3p_{\frac{1}{2}}$	0.00123(8)
1768(1)	$(1/2^-, 3/2^-)$	0.0082(8)	$3p_{\frac{1}{2}}$	0.0026(1)
1776(2)	$(5/2^-, 7/2^-)$	0.0063(8)	$2f_{\frac{5}{2}}$	0.0063(4)
1789(1)	$5/2^-, 7/2^-$	0.023(2)	$2f_{\frac{5}{2}}$	0.0267(8)
1821(3)	$1/2^-, 3/2^-$	0.0054(7)	$3p_{\frac{1}{2}}$	0.00101(8)
1830(2)	$1/2^-, 3/2^-$	0.0059(9)	$3p_{\frac{1}{2}}$	0.00157(9)
1857(1)	$5/2^-, 7/2^-$	0.1(6)	$2f_{\frac{5}{2}}$	0.117(3)
1882(1)	$1/2^-, 3/2^-$	0.028(2)	$3p_{\frac{1}{2}}$	0.0046(1)
1893(3)		0.0025(6)		
1927(2)		0.0062(8)		
1937(1)		0.022(2)		
1956(1)	$5/2^-, 7/2^-$	0.109(8)	$2f_{\frac{5}{2}}$	0.098(2)
1971(1)	$1/2^-, 3/2^-$	0.028(2)	$3p_{\frac{1}{2}}$	0.0069(2)
1978(1)	$5/2^-, 7/2^-$	0.021(2)	$2f_{\frac{5}{2}}$	0.0238(9)
1991(3)	$1/2^-, 3/2^-$	0.0056(8)	$3p_{\frac{1}{2}}$	0.0013(1)
1999(2)	$5/2^-, 7/2^-$	0.011(1)	$2f_{\frac{5}{2}}$	0.0109(5)
2009(1)	$13/2^+$	0.02(2)	$13i_{\frac{13}{2}}$	0.34(1)
2040(1)	$5/2^-, 7/2^-$	0.044(3)	$2f_{\frac{5}{2}}$	0.040(1)
2048(4)	$(1/2^-, 3/2^-)$	0.0063(9)	$3p_{\frac{1}{2}}$	0.0012(1)
2064(2)		0.006(1)		
2089(3)	$5/2^-, 7/2^-$ $1/2^-, 3/2^-$	0.038(3)	$2f_{\frac{5}{2}}$ $3p_{\frac{1}{2}}$	0.0064(5) 0.0076(5)
2130(1)	$9/2^-$	0.035(3)	$1h_{\frac{9}{2}}$	0.32(1)
2142(2)	$(1/2^-, 3/2^-)$	0.014(2)	$3p_{\frac{1}{2}}$	0.0032(1)
2157(3)	$(1/2^-, 3/2^-)$	0.007(1)	$3p_{\frac{1}{2}}$	0.00149(9)
2175(2)	$5/2^-, 7/2^-$	0.108(6)	$2f_{\frac{5}{2}}$	0.100(2)
2218(2)	$5/2^-, 7/2^-$	0.164(9)	$2f_{\frac{5}{2}}$	0.147(3)
2236(2)	$1/2^-, 3/2^-$	0.018(3)	$3p_{\frac{1}{2}}$	0.0037(1)
2248(2)		0.007(1)		
2259(4)		0.0018(5)		
2275(2)	$5/2^-, 7/2^-$	0.05(4)	$2f_{\frac{5}{2}}$	0.048(1)
2328(3)		0.008(1)		
2356(3)	$5/2^-, 7/2^-$	0.033(2)	$2f_{\frac{5}{2}}$	0.0283(8)
2377(3)	$5/2^-, 7/2^-$	0.014(2)	$2f_{\frac{5}{2}}$	0.0106(4)
2411(3)	$5/2^-, 7/2^{-\,c}$ $13/2^+$	0.021(1)	$2f_{\frac{5}{2}}$ $1i_{\frac{13}{2}}$	0.0083(3) 0.214(7)
2424(5)	$(1/2^-, 3/2^-)$	0.0033(8)	$3p_{\frac{1}{2}}$	0.0007(1)
2444(5)		0.0027(8)		
2459(4)	$5/2^-, 7/2^{-\,c}$	0.013(2)	$2f_{\frac{5}{2}}$	0.0115(4)
2508(5)	$5/2^-, 7/2^-$	0.039(3)	$2f_{\frac{5}{2}}$	0.0300(8)
2522(5)	$1/2^-, 3/2^-$	0.016(1)	$3p_{\frac{1}{2}}$	0.00158(9)
2539(6)	$(1/2^-, 3/2^-)$	0.0087(9)	$3p_{\frac{1}{2}}$	0.00164(9)
2570(6)	$5/2^-, 7/2^-$	0.037(3)	$2f_{\frac{5}{2}}$	0.0303(8)
2585(6)	$(1/2^-, 3/2^-)$	0.010(1)	$3p_{\frac{1}{2}}$	0.00139(8)
2672(7)		0.008(1)		
2686(9)		0.0012(6)		
2720(8)		0.02(3)		
2751(9)		0.005(1)		
2774(9)	$(1/2^-, 3/2^-)$	0.007(1)	$3p_{\frac{1}{2}}$	0.00090(8)
2800(10)		0.006(1)		
2847(11)		0.0047(9)		
2868(11)		0.017(2)		
2912(12)		0.004(1)		
2969(14)		0.008(2)		

the neighboring 699-keV level. The angular distribution is consistent with an $\ell = 3$ transfer, leading to the assignment of the spin-parity of this level as $\frac{5}{2}^-$ or $\frac{7}{2}^-$.

5. 759- and 825-keV levels

Levels at 759 and 825 keV, found in the earlier (d, p) transfer reaction [33], did not have assigned ℓ transfers. These levels were also observed in the present (d, t) work thus confirming their existence. For the 759-keV level, the $\ell = 3$ assignment is favored, leading to a spin assignment of $\frac{5}{2}^-$ or $\frac{7}{2}^-$. For the 825-keV level, the angular distribution is rather featureless but possesses the best agreement with an $\ell = 1$ angular distribution leading to a $\frac{1}{2}^-$ or $\frac{3}{2}^-$ assignment.

6. 1005- and 1108-keV levels

Levels previously observed at 1005 and 1108 keV in the (d, t) reaction [33] did not have assigned ℓ transfer values. In the present study, the ℓ transfer for the 1005-keV level is inconclusive. This level was observed in the (n, γ) reaction, as well as the (γ, γ') reaction, strongly favoring a $1/2^-$ or $3/2^-$ assignment. For the 1108-keV level, the angular distribution is consistent with an $\ell = 3$ transfer, leading to the spin-parity assignment of $\frac{5}{2}^-$ or $\frac{7}{2}^-$.

7. 1223- and 1230-keV levels

A level at 1230 keV was not conclusively assigned in earlier studies [14]. The neighboring level at 1223 keV was assigned as a probable doublet in the transfer work of Moyer [33]. In the present study, a doublet of states, at 1223.0(5) and 1229.5(3) keV, were successfully resolved. The angular distribution observed for the 1223-keV level is consistent with an $\ell = 1$ transfer resulting in the spin-parity assignment of as $\frac{1}{2}^-$ or $\frac{3}{2}^-$. The 1230-keV level is consistent with an $\ell = 3$ transfer yielding a spin-parity assignment of $\frac{5}{2}^-$ or $\frac{7}{2}^-$.

8. 1300-keV level

A new level at 1300(1) keV was observed to be very weakly populated in the (d, t) reaction. Its angular distribution could not be obtained at forward angles due to the presence of an impurity peak. The observed data are consistent with either an $\ell = 1$ or $\ell = 3$ transfer, leading to spin assignment in the range of $\frac{1}{2}^-$–$\frac{7}{2}^-$; however, we see a slight preference for the $\ell = 3$ assignment and thus Table III lists the spectroscopic strength due to $f_{5/2}$ transfer.

9. 1348-keV level

A new level is observed at 1347.8(7) keV that was populated with an angular distribution assigned as $\ell = 1$, leading to the spin assignment of $\frac{1}{2}^-$ or $\frac{3}{2}^-$.

10. 1355-keV level

The level at 1355(1) keV was observed to be very weakly populated in the present (d, t) reaction. It is tempting to associate it with the level at 1358.9 keV observed in the (n, γ) reaction [34], although the energy observed is a very poor match. The present angular distribution at forward angles was compromised due to the presence of impurity peaks. The observed angular distribution data are inconclusive; however, a slightly better fit is achieved with an $\ell = 3$ distribution than with $\ell = 1$. We thus tentatively suggest that it has spin-parity of $\frac{5}{2}^-$ or $\frac{7}{2}^-$.

11. 1362-keV level

A new level is observed at 1362.0(4) keV. The angular distribution is consistent with an $\ell = 6$ transfer, presumably from the $1i_{\frac{13}{2}}$ shell, leading to the spin-parity assignment of this level as $\frac{13}{2}^+$.

12. 1512- and 1531-keV levels

New levels are observed at 1512(1) and 1531(1) keV that are rather weakly populated. Their angular distributions appear to be inconsistent with any distribution except for $\ell = 1$, and thus we assign them as spin-parity $\frac{1}{2}^-$ or $\frac{3}{2}^-$ states.

13. 1566-keV level

A level was observed at 1565.5(7) keV. In the previous (d, t) reaction work [33], a state was tentatively assigned at 1561(6) keV whose angular distribution could not be obtained. We associate the present level at 1566 keV with the previously observed level at 1561 keV. In the present work, the angular distribution could be obtained and is assigned as an $\ell = 6$ transfer, leading to the $\frac{13}{2}^+$ assignment.

14. 1629-keV level

A new level was observed at 1629 keV. The angular distribution for its population was inconclusive, although we favor assigning it as an $\ell = 3$ transfer, leading to a tentative assignment of $\frac{5}{2}^-$ or $\frac{7}{2}^-$.

15. 1645- and 1653-keV levels

We observe a peak at 1645(1) keV that possesses an angular distribution that is assigned as an $\ell = 3$ transfer. A very close-lying state is also observed at 1652.5(6) keV that is strongly populated with an $\ell = 1$ transfer. The previous transfer studies [33] observed a level at 1649(7) keV in the (d, t) reaction and 1651(7) keV in the (d, p) reaction. The weaker-populated 1645-keV level was not observed.

16. 1686-keV level

The previous (d, t) study [33] observed a level at 1686(7) keV, but the transferred ℓ value could not be assigned. In the present work, a level at 1686.6(7) keV is observed with an angular distribution that is assigned as an $\ell = 3$ transfer, thus implying the spin-parity is $\frac{5}{2}^-$ or $\frac{7}{2}^-$.

17. 1735- and 1741-keV levels

A weakly populated doublet of states is observed at 1735(2) and 1741(3) keV. The latter level has an angular distribution for its population that is fit well with an $\ell = 1$ transfer, yielding a spin-parity of $\frac{1}{2}^-$ or $\frac{3}{2}^-$. This level matches well the known level at 1744.2(5) keV [14]. The 1735(2)-keV level has a very incomplete angular distribution, and thus a transferred ℓ value cannot be assigned. This level may correspond to the known level at 1731.8(7) keV [14] is assigned as a $\frac{1}{2}$ or $\frac{3}{2}$ state, which would favor an $\ell = 1$ transfer.

18. 1768-, 1776-, and 1789-keV levels

A triplet of states is observed at 1768(1), 1776(2), and 1789(1) keV. Of the three levels, the 1789-keV state is populated the strongest and a definite $\ell = 3$ transfer assignment can be made leading to its spin-parity of $\frac{5}{2}^-$ or $\frac{7}{2}^-$. The remaining levels of the triplet have much weaker population, and while not definitive, we favor an $\ell = 1$ transfer assignment for the 1768-keV level due to its relatively large cross section at forward angles and an $\ell = 3$ transfer for the level at 1776 keV due to its much weaker cross section at forward angles. Only one level in this excitation energy region at 1780.9(5) keV has been reported in the (n, γ) reaction [34].

19. 2089-keV levels

A doublet of states, not previously known [14], was observed at 2089 keV, and was assigned on the basis that the angular distribution appears to have both $\ell = 1$ and three transfer components. The spectroscopic factors listed in Table III are resulting from a two-component fit to the angular distribution.

20. 2130-keV level

A new level at 2130 keV was observed. The DWBA analysis is consistent with an $\ell = 5$ transfer from the $1h_{\frac{9}{2}}$ shell, assigning the spin-parity of this level as $\frac{9}{2}^-$. This was the only $\ell = 5$ transition firmly identified in the present work.

21. 2411-keV level

A level at 2411 keV was found in the earlier (d, t) transfer reaction [33], but with an unassigned ℓ transfer. This level was also observed by a ^{198}Hg(n, γ) reaction performed by Lone *et al.* [34]. They assigned the spin-parity of the level to be $\frac{1}{2}^{\pm}$, $\frac{3}{2}^{\pm}$, or $\frac{5}{2}^+$. In this work, the DWBA analysis is consistent with a combined $\ell = 3 + 6$ transfer, indicating a doublet of levels with I^π of $\frac{5}{2}^-$ or $\frac{7}{2}^-$ and $\frac{13}{2}^+$. The disagreement with the results of the neutron capture study suggests either an incorrect spin-parity asssignment or the possible existence of a third level near 2411 keV with the low-spin level not populated in the (d, t) transfer reaction.

22. 2459-keV level

This level was found in earlier (d, p) transfer-reaction experiments performed by Moyer [33], but without an assigned ℓ transfer. A level at 2462.1 keV was observed in the ^{198}Hg(n, γ) reaction performed by Lone *et al.* [34]. They assigned the spin of the level to be $\frac{1}{2}$ or $\frac{3}{2}$. In this work, the DWBA analysis is consistent with an $\ell = 3$ transfer, leading to the assignment of the spin-parity of this level as $\frac{5}{2}^-$ or $\frac{7}{2}^-$. As with the 2411-keV level, the discrepancy leads to the suggestion of a doublet of levels at 2459(4) and 2462.1 keV.

23. Summary of new $\ell = 1$ *assignments*

In total, eight new $\ell = 1$ transfers were assigned at 1348, 1512, 1531, 1830, 1882, 1991, 2236, and 2522 keV. The resulting angular distributions for six of these levels have unambiguous $\ell = 1$ transfers, assigned to be from the $3p_{\frac{1}{2},\frac{3}{2}}$ orbitals, leading to assigning the spin-parity of these levels as $\frac{1}{2}^-$ or $\frac{3}{2}^-$. The two levels at 1991 and 2522 keV have weaker cross sections but appear to be dominated by $3p_{\frac{1}{2},\frac{3}{2}}$ components. Several other levels have inconclusive angular distributions but are favored to be $\ell = 1$ and thus are tentatively assigned as $\frac{1}{2}^-$ or $\frac{3}{2}^-$.

24. Summary of new $\ell = 3$ *assignments*

Six new $\ell = 3$ transfers were observed to levels at 723, 1645, 1789, 1978, 1999, and 2508 keV. The angular distributions show strong agreement with $2f_{\frac{5}{2},\frac{7}{2}}$ components for four of these levels, assigning the spin-parity of these levels as $\frac{5}{2}^-$ or $\frac{7}{2}^-$. The two levels at 1645 and 1999 keV have tentative assignments of $\frac{5}{2}^-$ or $\frac{7}{2}^-$ based on their weaker and incomplete angular distributions.

25. Summary of new $\ell = 6$ *assignments*

Four new levels at 1362, 1566, 2009, and 2411 keV were identified as having $\ell = 6$ transfers from the $1i_{\frac{13}{2}}$ shell, giving spin-parity assignments of $\frac{13}{2}^+$. The level at 1566 keV identified in the present work may correspond to a level observed at 1561(6) keV, and the level at 2411 keV is part of an unresolved doublet.

Figure 9 displays the measured strengths to individual states plotted against their excitation energy. As can be seen, the $\ell = 1$ strength is concentrated at low excitation energies, below 500 keV, with the main remaining small fragments clustered between 1.2 and 1.5 MeV. The $\ell = 3$ strength is somewhat more fragmented, with the main contributions below 1.5 MeV. The $\ell = 6$ strength is mostly concentrated in the first $13/2^+$ state at 532 keV and appears to monotonically decrease with excitation energy.

V. DISCUSSION

A. Theoretical calculations

Calculations of the excitation energy spectrum and spectroscopic strengths were performed as outlined in Ref. [10]. The model space consisted of the $0h_{9/2}$, $1f_{7/2}$, $1f_{5/2}$, $2p_{3/2}$, $2p_{1/2}$, and $0i_{13/2}$ orbitals for the neutrons and the $0g_{7/2}$, $1d_{5/2}$, $1d_{3/2}$, $2s_{1/2}$, and $0h_{11/2}$ orbitals for the protons. The calculations used the Kuo-Herling interaction, originally developed by the G-matrix approach using the Hamada-Johnston potential. However, some of the two-body matrix elements were fitted to the experimental data of ^{206}Pb, ^{206}Tl, and ^{206}Hg. The shell-model calculations were performed to obtain the 50 lowest-energy states for each spin-parity of $J^\pi = 1/2^-$, $3/2^-$, $5/2^-$, $7/2^-$, $9/2^-$, and $13/2^+$.

As discussed in the next section, this experiment indicated that the single-particle $1/2^-$ state is concentrated in the ground state, whereas the $3/2^-$ and $5/2^-$ states are

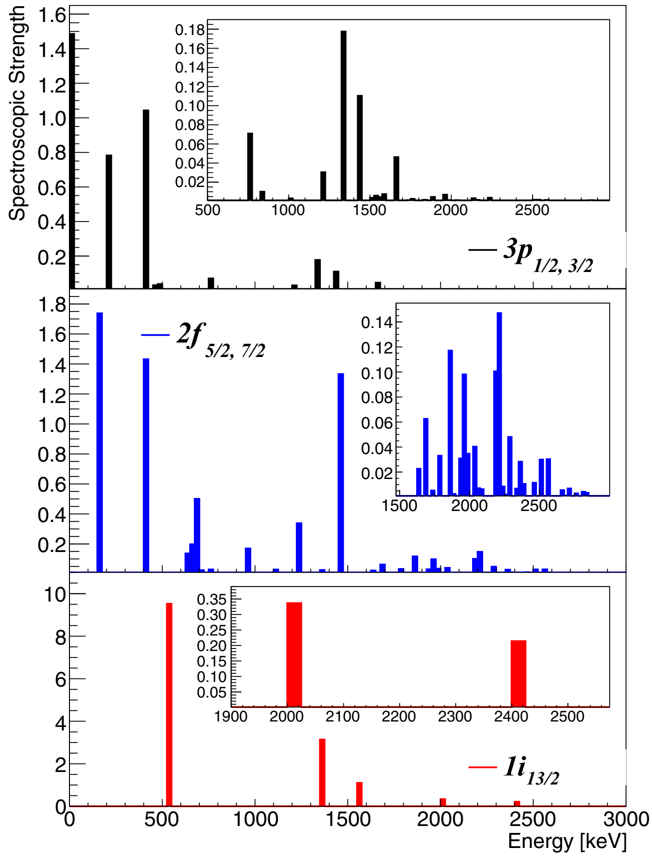

FIG. 9. Experimental spectroscopic strengths for $\ell = 1, 3,$ and 6 transfers up to 3 MeV in ^{199}Hg.

fragmented. This result is consistent with the discussion based on the $B(E2)$ values in Ref. [10]. The single-particle nature of the ground state indicate a significant contribution to the nuclear Schiff moment [35].

B. Comparison with experimental results

Table IV combined with Table I of the Supplemental Material [36] lists the results of the calculations up to an excitation

TABLE IV. Results of the theoretical calculations for levels below 1.5 MeV excitation energy and $J^\pi = 1/2^-, 3/2^-, 5/2^-, 7/2^-, 9/2^-$, and $13/2^+$.

E (keV)	J^π	$S_{\ell j}$
0	$1/2^-$	0.928
106	$5/2^-$	2.715
180	$3/2^-$	1.235
332	$3/2^-$	0.663
454	$3/2^-$	0.205
458	$1/2^-$	0.051
470	$5/2^-$	0.666
511	$13/2^+$	8.237
591	$7/2^-$	1.944
685	$5/2^-$	0.009
689	$9/2^-$	0.063
711	$7/2^-$	0.042
746	$3/2^-$	0.024
847	$5/2^-$	0.116
960	$7/2^-$	0.0003
1068	$3/2^-$	0.522
1086	$5/2^-$	0.012
1087	$7/2^-$	2.218
1124	$7/2^-$	0.502
1144	$9/2^-$	0.0017
1161	$1/2^-$	0.054
1306	$5/2^-$	0.012
1318	$3/2^-$	0.040
1319	$7/2^-$	0.197
1343	$9/2^-$	0.030
1353	$1/2^-$	0.0017
1371	$3/2^-$	0.0001
1376	$9/2^-$	0.005
1386	$5/2^-$	0.013
1431	$5/2^-$	0.084
1434	$7/2^-$	0.025
1436	$1/2^-$	0.007
1443	$13/2^+$	0.567
1463	$3/2^-$	0.020
1485	$5/2^-$	0.019

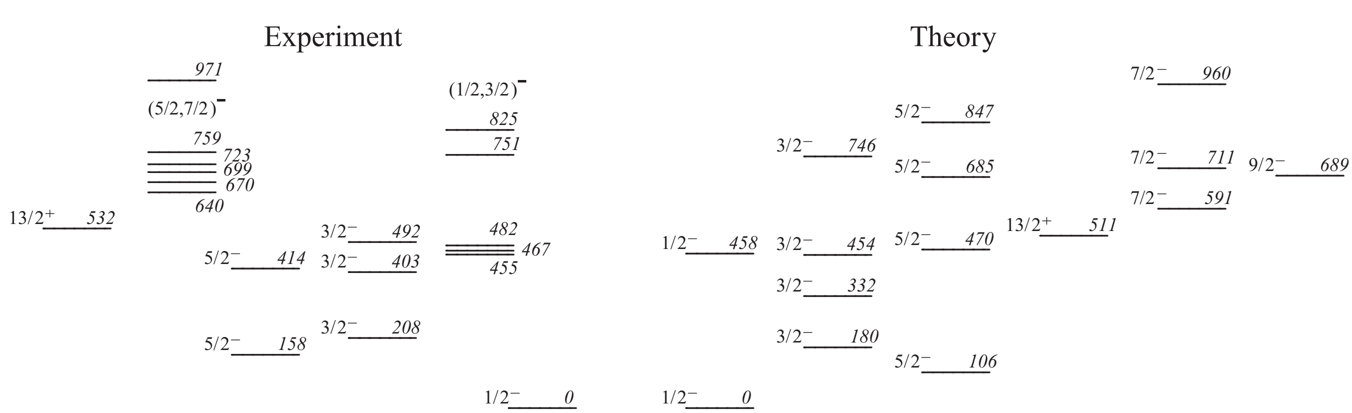

FIG. 10. Experimental levels (left) and theoretical levels (right) for ^{199}Hg. Levels up to 1-MeV excitation energy only are shown. For the observed levels with firm spin-parity assignments, they are written on the levels. Levels with uncertain spin-parity assignments are drawn under the possible values.

energy of 2.9 MeV and a maximum spin of $13/2^+$. It should be noted that in the comparison of the experimental and theoretical results, no renormalization of the spectroscopic strengths has been employed as will be discussed further below. A comparison of the experimental and theoretical level schemes is shown in Fig. 10 displaying all levels below 1-MeV excitation energy. As can be seen, more states are observed at low energies than are predicted. As was pointed out in Ref. [10], the adjacent even-even nuclei, for example ^{200}Hg, are known to be oblate deformed. One can thus expect that the low-lying states reflect the rotational character as evidenced by the enhanced $B(E2)$ values both observed and predicted for transitions between the low-lying states. From the Nilsson model, for oblate deformations we expect to observe the $\nu 1/2^-[521]$, $\nu 5/2^-[503]$, and $\nu 3/2^-[512]$ orbitals at low energies. Involving mainly the $p_{3/2}$ and $f_{5/2}$ spherical configurations, these Nilsson orbitals mix strongly and could account for many of the levels below 500 keV. The collective character of the states was reproduced by the LSSM calculations [10] even with the limitation of one-particle-one-hole excitations of the ground state.

The $I^\pi = \frac{1}{2}^-$ ground state was observed to be populated with a strength of $S = 1.49$, in excellent agreement with the calculations that also predict the ground state to be $\frac{1}{2}^-$ and with $S = 0.928$. The large experimental strength indicates that the ^{200}Hg ground state has a greater occupation of the $3p_{1/2}$ orbital than in the calculations. No other $1/2^-$ state is firmly identified in the experimental level scheme. The calculations predict that a $\frac{1}{2}^-$ state exists at 458 keV with $S = 0.051$, and all other higher-lying $\frac{1}{2}^-$ states are predicted to have negligible populations. Experimentally, there are three levels clustered near 480 keV that all have rather weak populations that could be candidates for the first excited $\frac{1}{2}^-$ state, but the current data do not permit us to identify which.

The first excited state observed is a $\frac{5}{2}^-$ state at 158 keV with $S = 1.74$, which is reproduced well in the calculations with a predicted excitation energy of 106 keV and $S = 2.715$. This is followed by two $\frac{3}{2}^-$ states observed at 208 and 403 keV with $S = 0.78$ and $S = 1.04$, respectively. In the calculations, there are three $3/2^-$ states predicted below 500 keV, all with significant strength. Experimentally, the three additional $\frac{1}{2}^-$ or $\frac{3}{2}^-$ states observed below 500 keV are all rather weakly populated. In fact, the next possible state observed with an $\ell = 1$ strength greater than 0.1 is the $(\frac{1}{2}^-, \frac{3}{2}^-)$ level at 1328 keV. The second $\frac{5}{2}^-$ state at 413 keV is also observed to be strongly populated, with $S = 1.43$, and is reproduced well in the calculations with an energy of 470 keV and $S = 0.67$. The $\frac{13}{2}^+$ state at 532 keV has a very strong $\ell = 6$ strength, with $S = 9.5$. In the calculations, the first $\frac{13}{2}^+$ state is predicted at 511 keV with $S = 8.2$. The second $\frac{13}{2}^+$ state is observed at 1362 keV with $S = 3.1$ and is calculated at 1443 keV with $S = 0.57$. This experimental state may be considered a match with the third predicted $\frac{13}{2}^+$ state at 1600 keV with $S = 2.21$. We note that due to the low intrinsic cross section for $\ell = 6$ transfers, states with small spectroscopic strengths may go undetected.

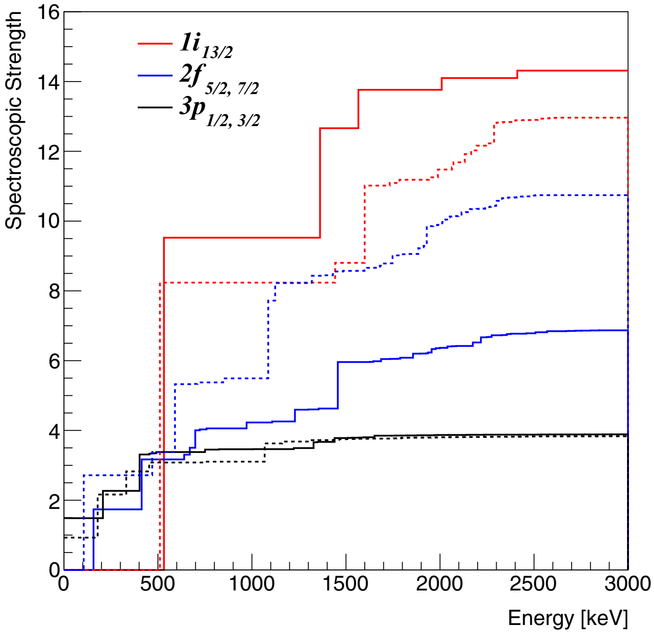

FIG. 11. Cumulative sum of the experimental spectroscopic strengths (solid lines) compared with the theoretical calculations (dashed lines) as a function of excitation energy for the $\ell = 1$ (p shell), $\ell = 3$ (f shell), and $\ell = 6$ (i shell) transfers up to 3 MeV.

Since there are many states observed with uncertain spin assignments, we find it more useful to consider the sum of the spectroscopic strengths as a function of the excitation energy, where we take the total $\ell = 1$ and $\ell = 3$ strengths. This is shown in Fig. 11. The $\ell = 1$ strength distribution is reproduced extremely well both in magnitude and trend. The $i_{13/2}$ strength distribution is also very well reproduced, although slightly more strength is observed experimentally than calculated. By far the largest deviation occurs for the $\ell = 3$ strength, with significantly more strength calculated than observed, and large amounts of strength predicted near 600 and 1100 keV and experimentally only moderate amounts near 700 and 1500 keV.

C. Summed spectroscopic strengths

The summed strength of neutron stripping (or neutron adding when referring to the target, G_j^+) and pickup (or neutron removing, G_j^-) reactions acting on a target A for the transfer of a particle of a given orbit with angular momentum j can be expressed as

$$(2j+1)N_j = G_j^+ + G_j^-, \tag{5}$$

where

$$G_j^+ = \sum_i (2j+1)C^2 S_i^+, \quad G_j^- = \sum_i C^2 S_i^- \tag{6}$$

and the summation extends over all final states i. The C^2 factors are squares of isospin Clebsch-Gordan coefficients, and for the neutron stripping reaction, $C^2 = 1$. In the present case, we also take $C^2 = 1$ for the pickup reaction in the approximation that the corresponding proton orbitals forming

TABLE V. Sum of the spectroscopic strengths observed in the (d,t) pickup reaction (this work) and the (d,p) stripping reaction [33]. Results are shown for the total p and f shell strength, and the $i_{13/2}$ shell. The spectroscopic strengths in the (d,t) reaction have an estimated 15% systematic uncertainty included that dominates the statistical uncertainties. The spectroscopic strengths in the (d,p) reaction have been assigned with a 25% uncertainty (see text for details). The last line in the table gives the total expected degeneracy of the shells. No renormalizations of the observed strengths have been applied.

	Spectroscopic strengths ($S_{\ell j}$)		
Experiment	$\Sigma\, p_{1/2,3/2}$	$\Sigma\, f_{5/2,7/2}$	$\Sigma\, i_{13/2}$
^{200}Hg(d,t)	3.0(6)	6.9(10)	14.3(21)
^{200}Hg(d,p) [33]	2.5(6)	3.4(9)−4.8(12)	0.0
Σ	6.4(8)	10.3(13)−11.7(16)	14.3(21)
$2J+1$	6.00	14.00	14.0

the isobaric analog states are unoccupied (see e.g., Ref. [37] for a discussion). Thus, we form the sum

$$(2j+1)N_j = \sum_i (2j+1)S_i^+ + \sum_i S_i^-. \qquad (7)$$

The N_j factor is a normalization factor explored in Refs. [38–40], and for single-nucleon transfer reactions has been determined to be 0.55 ± 0.10, although incorporating variations in choices of DWBA parametrizations leads to a higher uncertainty of approximately 0.2 [39].

Table V outlines the summed spectroscopic strengths for the (d,t) pickup reaction of this work, and the (d,p) stripping reaction performed by Moyer [33], without the application of the normalization factor N_j. The uncertainties on the spectroscopic strengths for the (d,p) reaction were cited in Ref. [33] to be perhaps as large as 50% with a significant contribution arising from the uncertainties in absolute cross sections. However, we generally find very good agreement with the (d,t) strengths extracted for ^{200}Hg(d,t) reaction. For example the strength reported for the ground state was $S = 1.5$ [33] compared with our 1.49(3). For the $\ell = 3$ and $\ell = 6$ transitions to the 158- and 532-keV states, Moyer [33] reports strengths of 2.4 and 7.4, respectively, compared with our strengths of 1.74(4) (78% of the previous value) and 9.5(2) (138% of the previous value). We conclude that the differences in the extracted strengths are largely due to differences in the reaction modeling rather than errors in the absolute cross sections reported by Moyer [33]. We thus take a reduced uncertainty of ±25% on the (d,p) strengths reported by Moyer [33]. For the $\ell = 3$ (d,p) strength, we treat the two peaks reported by Moyer [33] at 1946 and 2081 keV that were fit as mixtures of f and $g_{9/2}$ transfers as more unreliable; without their contributions we have a sum of 3.4(9), and with, 4.8(12).

The sum rules for the $p_{1/2,3/2}$ shells in the two reactions indicate all the spectroscopic strength has been accounted for. In both reactions, the majority of the strength lies low in energy. In the (d,t) pickup reaction, roughly 85% of the total observed strength is concentrated in the first three states under 500 keV. The sum rule for the $i_{13/2}$ shell is entirely accounted for in the (d,t) pickup reaction, indicating that this shell is completely filled. There was some possible observed $\ell = 6$ strength in the (d,p) reaction [33]; however, these transfers were to levels high in energy (>3.8 MeV) and corresponded to the $i_{11/2}$ shell, above the $N = 126$ shell gap. The sum rules for the $f_{5/2,7/2}$ shells remains unfilled, implying a fragmentation in (d,t) strength above 3 MeV. It should be noted that if we adopted a quenching factor of 0.6(2), we would expect a summed strength of 8.0(2.8), whereas the observed strength is in the range of 10.3(13) to 11.7(16).

Finally, a single $\ell = 5$ transfer was observed in the (d,t) pickup reaction at 2130 keV (see Fig. 7). No complementary $\ell = 5$ transfer was observed in the (d,p) or (d,t) reaction performed by Moyer [33]. The relatively high energy of this level, and the lack of observation in the (d,p) stripping reaction is consistent with this subshell lying deep beneath the Fermi surface.

As outlined in Ref. [10], the nuclear Schiff moment of the $[\frac{1}{2}^-]_2$ state is predicted to be significantly quenched compared to that of the ground state. Any mixing of the $[\frac{1}{2}^-]_1$ and $[\frac{1}{2}^-]_2$ states would reduce the Schiff moment of the ground state and thus also reduce the sensitivity of the ^{199}Hg EDM measurements. Under the assumption that the $(\frac{1}{2}^-, \frac{3}{2}^-)$ level at 455 keV is the $[\frac{1}{2}^-]_2$ state, we can place a limit on its possible mixing provided that the unperturbed $[\frac{1}{2}^-]_2$ state has no intrinsic single-particle spectroscopic strength. Then, in a two-state mixing scenario the ratio of the spectroscopic strengths $S(455)/S_{\mathrm{gs}} = 0.0254(8)/1.49(3) = \alpha^2/(1-\alpha^2)$ with α the mixing amplitude. Solving, we have $\alpha^2 = 1.7(1)\%$. However, this must be considered only as a crude estimate due to the assumption of zero intrinsic single-particle strength for the unperturbed $[\frac{1}{2}^-]_2$ state. Measurements of absolute transition rates of the low-lying levels in ^{199}Hg would provide important complementary information, as would the magnetic moment of the $[\frac{1}{2}^-]_2$ level.

VI. SUMMARY

The motivation of this experiment was to probe the single-particle natures of states in ^{199}Hg via the (d,t) neutron pickup reaction. We performed the ^{200}Hg$(d,t)^{199}$Hg reaction using 22 MeV deuteron beams obtained from the Maier-Leibnitz Laboratory, and analyzed the reaction products with a Q3D magnetic spectrograph. In total, 93 levels were assigned. New spin-parity assignments were made for 16 previously established levels. These levels were observed in the transfer reaction experiments performed by Moyer [33]; however, the ℓ transfer was not previously determined. In the present work the ℓ transfer was determined, giving possible spin-parity assignments. Additionally, 52 previously unobserved levels were identified of which 22 have confidently assigned transfer ℓ values giving possible spin-parity assignments. The results of the experiment are compared to large-scale shell-model calculations that reproduce the observed strengths very well, giving confidence in the calculation of the ^{199}Hg Schiff moment.

ACKNOWLEDGMENTS

This work was supported in part by the Natural Sciences and Engineering Research Council of Canada. A special thanks to the target makers D. Frischke, H.-J. Maier, and J. Szerypo (Fakultät für Physik, Ludwig-Maximilians-Universität München). We used the KSHELL code [41] for the shell-model calculations. The numerical calculation was performed on the Oakforest-PACS supercomputer for Multidisciplinary Computational Sciences Project of Tsukuba University (xg18i035) and the Wisteria-O supercomputer at the CCS, University of Tsukuba. K. Yanase was supported by JSPS KAKENHI Grant No. JP22K14031.

DATA AVAILABILITY

The data that support the findings of this article are not publicly available upon publication because it is not technically feasible and/or the cost of preparing, depositing, and hosting the data would be prohibitive within the terms of this research project. The data are available from the authors upon reasonable request.

[1] T. E. Chupp, P. Fierlinger, M. J. Ramsey-Musolf, and J. T. Singh, Electric dipole moments of atoms, molecules, nuclei, and particles, Rev. Mod. Phys. **91**, 015001 (2019).

[2] N. Yamanaka, B. K. Sahoo, N. Yoshinaga, T. Sato, K. Asahi, and B. P. Das, Probing exotic phenomena at the interface of nuclear and particle physics with the electric dipole moments of diamagnetic atoms: A unique window to hadronic and semi-leptonic CP violation, Eur. Phys. J. A **53**, 54 (2017).

[3] B. Graner, Y. Chen, E. G. Lindahl, and B. R. Heckel, Reduced limit on the permanent electric dipole moment of ^{199}Hg, Phys. Rev. Lett. **116**, 161601 (2016).

[4] L. I. Schiff, Measurability of nuclear electric dipole moments, Phys. Rev. **132**, 2194 (1963).

[5] V. V. Flambaum and V. G. Zelevinsky, Enhancement of nuclear Schiff moments and time-reversal violation in atoms due to soft nuclear octupole vibrations, Phys. Rev. C **68**, 035502 (2003).

[6] N. Auerbach, V. V. Flambaum, and V. Spevak, Collective T- and P-odd electromagnetic moments in nuclei with octupole deformations, Phys. Rev. Lett. **76**, 4316 (1996).

[7] V. Spevak, N. Auerbach, and V. V. Flambaum, Enhanced T-odd, P-odd electromagnetic moments in reflection asymmetric nuclei, Phys. Rev. C **56**, 1357 (1997).

[8] K. Yanase, Screening of nucleon electric dipole moments in atomic systems, Phys. Rev. C **103**, 035501 (2021).

[9] J. Engel, J. L. Friar, and A. C. Hayes, Nuclear octupole correlations and the enhancement of atomic time-reversal violation, Phys. Rev. C **61**, 035502 (2000).

[10] K. Yanase and N. Shimizu, Large-scale shell-model calculations of nuclear Schiff moments of ^{129}Xe and ^{199}Hg, Phys. Rev. C **102**, 065502 (2020).

[11] H.-F. Wirth, H. Angerer, T. von Egidy, Y. Eisermann, G. Graw, and R. Hertenberger, New Q3D Focal Plane Detector with Cathode-strip Readout Became Operational, Technical Report, MLL Jahresbericht, 2000.

[12] P. E. Garrett, E. T. Rand, A. Diaz Varela, G. C. Ball, V. Bildstein, T. Faestermann, B. Hadinia, R. Hertenberger, D. S. Jamieson, B. Jigmeddorj, K. G. Leach, C. E. Svensson, and H.-F. Wirth, Direct reactions for nuclear structure required for fundamental symmetry tests, EPJ Web Conf. **123**, 03003 (2016).

[13] A. Heusler, G. Graw, R. Hertenberger, F. Riess, H.-F. Wirth, and P. von Brentano, On the Linearity of the Q3D Magnetic Spectrograph, Technical Report, MLL Jahresbericht, 2004.

[14] B. Singh, Nuclear data sheets for $A = 199$, Nucl. Data Sheets **108**, 79 (2007).

[15] F. James and M. Winkler, Minuit User's Guide, Technical Report, CERN, Geneva, 2004.

[16] P. R. Bevington and D. K. Robinson, *Data Reduction and Error Analysis for the Physical Sciences*, 3rd ed. (McGraw–Hill, New York, 2003).

[17] J. Kern, Computer analysis of nuclear spectra and γ-energy standards, Nucl. Instrum. Methods **79**, 233 (1970).

[18] I. J. Thompson, Coupled reaction channels calculations in nuclear physics, Comput. Phys. Rep. **7**, 167 (1988).

[19] I. J. Thompson and F. M. Nunes, *Nuclear Reactions for Astrophysics: Principles, Calculation and Applications of Low-energy Reactions* (Cambridge University Press, Cambridge, UK, 2009).

[20] W. W. Daehnick, J. D. Childs, and Z. Vrcelj, Global optical model potential for elastic deuteron scattering from 12 to 90 MeV, Phys. Rev. C **21**, 2253 (1980).

[21] H. An and C. Cai, Global deuteron optical model potential for the energy range up to 183 MeV, Phys. Rev. C **73**, 054605 (2006).

[22] J. Bojowald, H. Machner, H. Nann, W. Oelert, M. Rogge, and P. Turek, Elastic deuteron scattering and optical model parameters at energies up to 100 MeV, Phys. Rev. C **38**, 1153 (1988).

[23] Y. Han, Y. Shi, and Q. Shen, Deuteron global optical model potential for energies up to 200 MeV, Phys. Rev. C **74**, 044615 (2006).

[24] X. Li, C. Liang, and C. Cai, Global triton optical model potential, Nucl. Phys. A **789**, 103 (2007).

[25] V. Zerkin, Experimental Nuclear Reaction Data (EXFOR), https://www-nds.iaea.org/exfor/exfor.htm, accessed: 2015-07-01.

[26] N. Otuka, E. Dupont, V. Semkova, B. Pritychenko, A. Blokhin, M. Aikawa, S. Babykina, M. Bossant, G. Chen, S. Dunaeva, *et al.*, Towards a more complete and accurate Experimental Nuclear Reaction Data Library (EXFOR): International collaboration between Nuclear Reaction Data Centres (NRDC), Nucl. Data Sheets **120**, 272 (2014).

[27] J. B. A. England, L. Zybert, G. T. A. Squier, O. Karban, R. Zybert, J. M. Nelson, D. Barker, B. R. Fulton, M. C. Mannion, C. A. Ogilvie, *et al.*, Elastic scattering of 33 MeV tritons and isospin dependence of mass-3 optical potential, Nucl. Phys. A **475**, 422 (1987).

[28] D. Y. Pang, P. Roussel-Chomaz, H. Savajols, R. L. Varner, and R. Wolski, Global optical model potential for $A = 3$ projectiles, Phys. Rev. C **79**, 024615 (2009).

[29] A. J. Koning and J. P. Delaroche, Local and global nucleon optical models from 1 keV to 200 MeV, Nucl. Phys. A **713**, 231 (2003).

[30] I. J. Thompson (private communication, 2015).

[31] T. G. Pelham, Calculation of ^{7}Be$(d,t)^6$Be with Fresco, and investigation into resonant states of ^{6}Be, Ph.D.

thesis, Department of Physics, University of Surrey, Guildford, 2009.

[32] P. D. Kunz and E. Rost, The distorted-wave born approximation, in *Computational Nuclear Physics 2: Nuclear Reactions*, edited by K. Langanke, J. A. Maruhn, and S. E. Koonin (Springer, New York, 1993), pp. 88–107.

[33] R. A. Moyer, Deuteron-induced reactions on the even-even isotopes of mercury, Phys. Rev. C **5**, 1678 (1972).

[34] M. A. Lone, E. D. Earle, and G. A. Bartholomew, Resonance neutron capture in ^{198,199,201}Hg, Nucl. Phys. A **243**, 413 (1975).

[35] K. Yanase, N. Shimizu, K. Higashiyama, and N. Yoshinaga, Correlations between nuclear Schiff moment and electromagnetic measurements, Phys. Lett. B **841**, 137897 (2023).

[36] See Supplemental Material at http://link.aps.org/supplemental/10.1103/4r6p-prgy for the calculated levels above 1.5 MeV.

[37] S. V. Szwec, B. P. Kay, T. E. Cocolios, J. P. Entwisle, S. J. Freeman, L. P. Gaffney, V. Guimarães, F. Hammache, P. P. McKee, E. Parr, C. Portail, J. P. Schiffer, N. de Séréville, D. K. Sharp, J. F. Smith, and I. Stefan, Rearrangement of valence neutrons in the neutrinoless double- β decay of ^{136}Xe, Phys. Rev. C **94**, 054314 (2016).

[38] J. P. Schiffer, C. R. Hoffman, B. P. Kay, J. A. Clark, C. M. Deibel, S. J. Freeman, A. M. Howard, A. J. Mitchell, P. D. Parker, D. K. Sharp, *et al.*, Test of sum rules in nucleon transfer reactions, Phys. Rev. Lett. **108**, 022501 (2012).

[39] B. P. Kay, J. P. Schiffer, and S. J. Freeman, Quenching of cross sections in nucleon transfer reactions, Phys. Rev. Lett. **111**, 042502 (2013).

[40] T. Aumann, C. Barbieri, D. Bazin, C. Bertulani, A. Bonaccorso, W. Dickhoff, A. Gade, M. Gómez-Ramos, B. Kay, A. Moro, T. Nakamura, A. Obertelli, K. Ogata, S. Paschalis, and T. Uesaka, Quenching of single-particle strength from direct reactions with stable and rare-isotope beams, Prog. Part. Nucl. Phys. **118**, 103847 (2021).

[41] N. Shimizu, T. Mizusaki, Y. Utsuno, and Y. Tsunoda, Thick-restart block Lanczos method for large-scale shell-model calculations, Comput. Phys. Commun. **244**, 372 (2019).